ADVANCED FUNCTIONAL MATERIALS
www.afm-journal.de

Multifunctional Three-Dimensional T-Junction Graphene Micro-Wells: Energy-Efficient, Plasma-Enabled Growth and Instant Water-Based Transfer for Flexible Device Applications

*Shailesh Kumar, Timothy van der Laan, Amanda Evelyn Rider, Lakshman Randeniya, and Kostya (Ken) Ostrikov**

The "third-generation" 3D graphene structures, T-junction graphene micro-wells (T-GMWs) are produced on cheap polycrystalline Cu foils in a single-step, low-temperature (270 °C), energy-efficient, and environment-friendly dry plasma-enabled process. T-GMWs comprise vertical graphene (VG) petal-like sheets that seemlessly integrate with each other and the underlying horizontal graphene sheets by forming T-junctions. The microwells have the pico-to-femto-liter storage capacity and precipitate compartmentalized PBS crystals. The T-GMW films are transferred from the Cu substrates, without damage to the both, in de-ionized or tap water, at room temperature, and without commonly used sacrificial materials or hazardous chemicals. The Cu substrates are then re-used to produce similar-quality T-GMWs after a simple plasma conditioning. The isolated T-GMW films are transferred to diverse substrates and devices and show remarkable recovery of their electrical, optical, and hazardous NO_2 gas sensing properties upon repeated bending (down to 1 mm radius) and release of flexible trasparent display plastic substrates. The plasma-enabled mechanism of T-GMW isolation in water is proposed and supported by the Cu plasma surface modification analysis. Our GMWs are suitable for various optoelectronic, sesning, energy, and biomedical applications while the growth approach is potentially scalable for future pilot-scale industrial production.

1. Introduction

Owing to its unique electronic, optical, mechanical, and functional properties,[1] supported horizontal graphenes may potentially revolutionize the fields of flexible, transparent and ultra-light nanodevices,[2] from optoelectronics to sensors.[3,4] For several applications, graphenes in vertical orientations offer substantially enhanced functionalities,[5,6] mostly due to the very large surface areas and ultra-long open reactive edges of the vertical graphene sheets. Both the sheets and the edges may be used to accommodate a very high density of functional nanoparticles (e.g., quantum dots) and enable effective interactions (e.g., adsorption, desorption, immobilization, charge exchange, photo-excitation, etc.) with a broad range of species, from photons and electrons in optoelectronics to reactive ions in energy storage and peptides/proteins in biomedical applications.[7,8] Most of these interactions lead to the transfer of electric charges that need to be transported through the vertical sheets to the points of charge collection and subsequent transport to the external circuits.

Therefore, the ideal vertical graphenes should offer ultrafast charge transport through the low-defect vertical sheets as well as low-contact-resistance sites over the entire base edge, vertical planes, and the remaining edges. The charge transport may also be dramatically improved by internetworking the vertically oriented graphene sheets (for simplicity labelled VGs thereafter) through their vertical edges to form petal-like VGs (PVGs) as shown in **Figure 1**. Compared to substrate-supported VGs, PVGs offer better flexibility, optical transparency, charge transfer, are more light-weight, thus reprsesenting the "second-generation" of vertical graphenes with many far-going potential applications.[9–11] However, the PVG structures are most commonly formed via colloidal self-assembly of exfoliated and separated grapehene sheets. These three-dimensional (3D) PVG networks are very flexible in the x and y basal directions

Dr. S. Kumar, T. van der Laan, Dr. A. E. Rider, Dr. L. Randeniya, Prof. K. Ostrikov
Plasma Nanoscience Laboratories
CSIRO Materials Science and Engineering
P.O. Box 218, Lindfield, NSW 2070, Australia
E-mail: Kostya.Ostrikov@csiro.au
T. van der Laan, Dr. A. E. Rider, Prof. K. (Ken) Ostrikov
Plasma Nanoscience @ Complex Systems
School of Physics
University of Sydney
NSW 2006, Australia
Prof. K. (Ken) Ostrikov
School of Chemistry, Physics, and Mechanical Engineering
Queensland University of Technology
Brisbane, QLD 4000, Australia

DOI: 10.1002/adfm.201400992

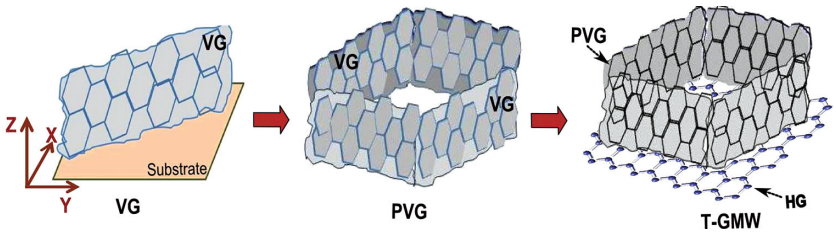

Figure 1. Schematics show the three "generations" of vertically oriented graphenes structures. a) Surface-supported vertically oriented graphenes (VG) with an individual[22] or maze-like[6] morphology. b) A petal-like VG (PVG)[9] structure is formed by self-assembly of few VGs. c) T-junction graphene micro-well (T-GMW) structure (current work) is formed by seemless integration of horizontal graphene (HG) and PVG layers.

(Figure 1) and may easily deform and compromise functionality upon substrate transfer. Due to the very high growth temperatures it is presently extremely challenging to grow them (e.g., using thermal chemical vapor deposition, CVD) directly onto (e.g., semiconductor) device locations.

A possible solution may be to first grow PVGs on a catalyst substrate and then transfer to the device. Unfortunatley, surface-supported PVG networks are most commonly produced using plasma-enhanced CVD (PECVD) on semiconductor substrates with thin oxide layers, and it is nearly impossible to separate the PVGs from the substrate without damaging both. Recent discovery of CVD and PECVD growth of horizontal graphenes on copper substrates, with several options for graphene film device transfer[12,13] open the unique, yet not materialized possibility to first grow one or more horizontal layers of horizontal graphenes (HG) on copper, and then bend and scroll the next few layers to extend vertically as shown in Figure 1. This unique possibility is demonstrated for the first time in this work.

We name the resulting 3D structures T-junction graphene micro-wells (T-GMWs) because of the fairly rigid T-junctions that form both between the adjacent VG sheets and between the VG base edges and the underlaying HG layers. In this way, the VG sheets interconnect into a PVG network that becomes rigid in the *x*-*y* plane and seemlessly integrates with the horizontal graphene support. The latter integration naturally further improves the charge collection from the VG sheets and potentially enables their ballistic transport to the external circuit through the HG layers. Moreover, the vertical scrolling of graphene sheets while retaining unscrolled horizontal layers enables good flexibility in the *z*-direction while preserving network rigidity in the *x*-*y* plane. The VG sheets form petal-like micrometer-sized wells with a "leak-free" bottom and an open top end, which makes them ideal containers with the storage capacity in the pico-to-femto-liter range. As such, the T-GMWs may be regarded as the "third-generation" vertical graphenes.

Therefore, here we report on the scalable fabrication of a high-quality, structurally rigid (in the *x*-*y* plane), yet flexible (in the *z* direction) 3D T-junction graphene micro-wells on cheap polycrystalline Cu foils in a customized single-step low-temparature plasma-enabled process. The T-junction integration of the vertical graphene sheets with the supporting horizontal graphene layers is achieved through a continuos single-step growth process without any wet-chemicals, binders, textures, or catalyst particles that are commonly used to create 3D hybrid micro- and nanostructures. The T-GMW films are not only optically transparent (76% at a wavelength of 550 nm), but also exhibit mechanical and structural integrity that remains almost unaltered upon large mechanical deformation repeated many times. Our plasma-enabled growth process only takes 3–5 minutes at a temperature of less than 270 °C. This is at least 50% more energy efficient than previously reported PECVD-based methods, which feature growth temperatures of 400–750 degrees,[6,13] while thermal CVD of graphenes on copper and other substrates usually requires 750–1000 degrees.[14] We also show that the thickness of the vertical graphene layers can be as small as 2–6 atomic layers, while the density of upwards- facing open ultra-long reactive graphene edges can exceed ~400 m/cm^2.

Moreover, we demonstrate a simple, water-based transfer of T-GMW films into virtually any, but particularly onto flexible transparent substrates, without any significant compromise to the integrity, morphology, or structure of the T-GMWs, while retaining the catalytic ability of the Cu substrates for further re-use. This is a substantial step-change compared to commonly used transfer methods that either rely on complex multi-step procedures and involve several sacrificial materials (e.g., polymer layers)[13,15] or complete etching of underlaying copper catalyst.[16] The latter methods not only use reactive and toxic chemicals such as $FeCl_3$ but also often decrease the graphene quality by introducing unwanted defects.

Our studies also reveal the mechanism of the water-based *decoupling* and *lift-off* of the T-GMW films through the plasma-specific modification of nanoscale crystallographic features of the polycrystalline Cu substrate surface at a very low temperature (<190 °C). These plasma-surface interactions not only activate the Cu surface for deposition of high-quality T-GMW films but also induce mutual repulsion of the underlaying HG layer and the copper substrate upon immersion in de-ionized (or common tap) water at room temperature (22 °C). This is a critical step towards a relatively cost-effective and environment-friendly transfer process, which is also material-efficient as it allows the copper substrate to be re-used many times for the fabrication of similar-quality T-GMW films. The transparent T-GMW-films were easily transferred to any chemically diverse targeted substrate (paper, polymer, glass, etc.) without using any polymeric coatings[16] and retained their properties after bending several times at 1 mm radius of curvature.

Finally, the transparent, conducting, and flexible T-GMW films were integrated into nanodevices and demonstrated a remarkable performance as NO_2 gas sensors at room temperature. We also show applicability of the graphene micro-wells as compartmentalized containers of virtually any chemicals or culture media including living cells, peptides/proteins with the pico-to-femto-liter storage capacity of individual wells.

We also demonstrate that PVG networks can also be grown directly on polycrystalline Cu substrates and show qualitatively similar basic features (low-temperature growth, water-based transfer, retention of functional properties upon bending and release) and NO_2 sensing responses. However, the properties

and performance of the novel T-GMW films always remain superior compared to PVG structures.

The PVGs and T-GMWs production processes are potentially scalable owing to the recently demonstrated roll-to-roll production of few-layer graphene films on Cu using microwave PECVD.[15] Importantly, these methods presently suffer from significantly lower graphene quality (compared to common thermal CVD and our plasma-based methods) and also use toxic $FeCl_3$ to dissolve Cu films to release the graphene films. Given that development of scaled-up batch and roll-to-roll processes is on our agenda, these recent advances suggest that our method is indeed potentially scalable and amenable for the future pilot-scale industrial production.

2. Results and Discussion

2.1. Plasma-Enabled Graphene Microwells

The schematic in **Figure 2**a shows a one-step, cost and energy-efficient growth process for high-quality T-GMW films. The films comprised of integrated networks of horizontal and vertical graphene sheets were grown on cheap polycrystalline Cu foils by directly exposing them to low-power (<700 W) CH_4 + H_2 + Ar plasmas. No external heating was used and the Cu-surface temperature in the range of 180–260 °C was achieved merely due to the plasma heating.[17] The high quality of the deposited films can be attributed to the plasma-assisted

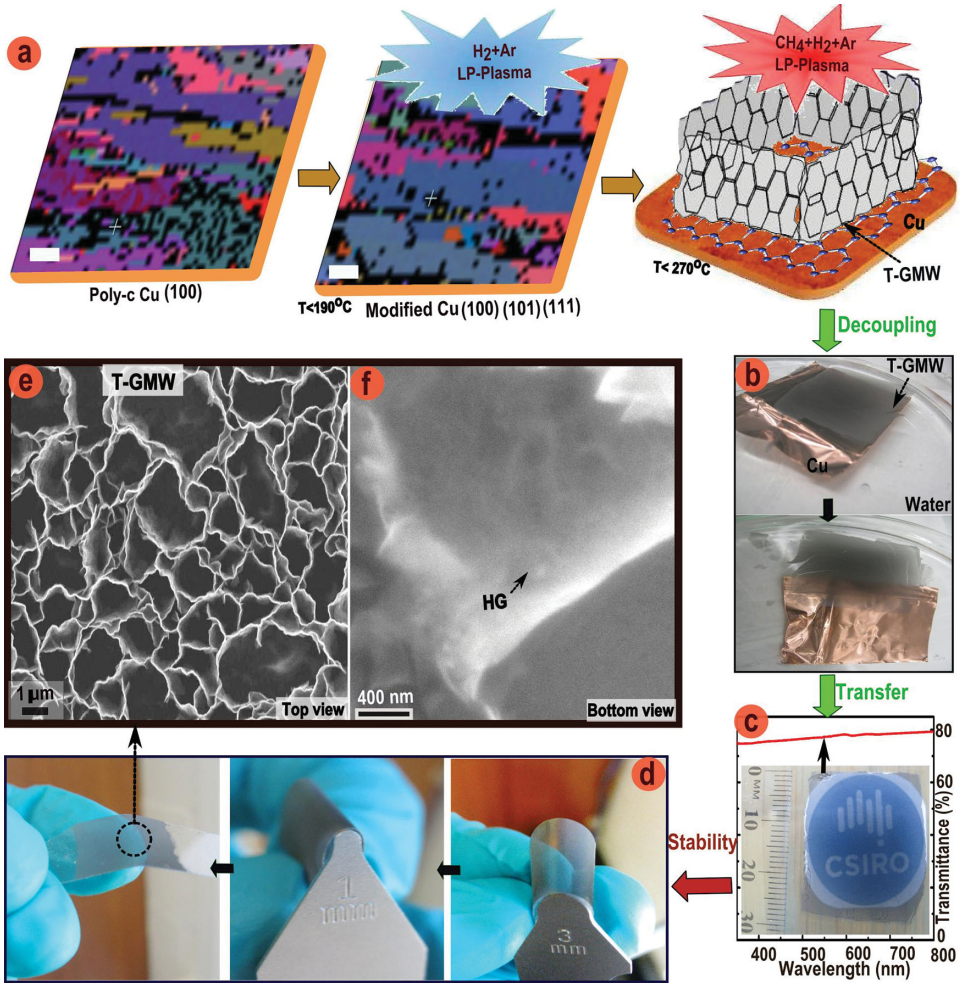

Figure 2. Plasma-enabled wet-chemical-/binder-free, highly integrated 3D vertical graphenes (T-GMWs) network, chemical-free (C-F) instant decopling, flexible substrate transfer and stability upon bending. a) Growth process of graphene micowells. EBSD mapping images show the crystal phase orientation on the surface of a polycrystalline Cu foil, which was originally dominated by the (100) phase and then modified by the H_2 + Ar plasma treatment to express predominant (101) and (111) phases even at the foil temperature <190 °C. After adding CH_4, the integrated T-GMW structures were grown at the foil temperature <270 °C. b) Digital optical images show that the T-GMW film is instantly decoupled, lifted-off from the foil and left floating on the water surface at room temperature (RT) after immersing into de-ionized water. As the process is chemical-free (C-F), the Cu foil was re-used to produce almost similar-quality T-GMW films. c) The T-GMW film after a transfer onto a polyethylene (PET) sheet shows ~76% transparency at wavelength of 550 nm. d) Digital photos show the 10th bending cycle of the T-GMW/PET films (bending from flat to the minimum radius of curvature of 1 mm). e-f) SEM images of a T-GMW film after the 10th cycle of bending, e) top-view SEM image shows highly integrated, petal-like vertical graphene network with a high density of graphitic edges ~400 m/cm^2, f) the bottom-view shows the HG layers underneath the vertical graphene networks. Unless specified, scale bars are 25 μm.

activation of the Cu surface. The crystal orientation of polycrystalline Cu surface (dominated by the (100) plane) was effectively modified after its exposure to H_2 + Ar plasmas for 90 seconds and an increase in (101) and (111) higher-index facets with larger grains on the surface was observed (Figure 2a, the electron backscattering diffraction (EBSD) images in the figure show z-plane of the foils). The surface temperature remained below 190 °C during the process. When CH_4 carbon precursor gas was mixed with H_2 and Ar after 90 seconds into the process, horizontal graphene layers integrated with petal-like vertical graphene layers were deposited on the foil surface (Figure 2e,f). However, when the Cu foil was directly exposed to CH_4 + H_2 + Ar plasmas in the absence of a H_2 + Ar pretreatment step, we have deposited PVG films (**Figure 3**h) with a relatively lower structural quality (and consequently, functional performance indicators, details below) compared to the T-GMW films. The direct exposure to methane plasmas did not produce these nanostructures on the Cu surface. Thus, the higher-index facets of Cu (which emerge as a result of the H_2 + Ar plasma exposure) enhance the nucleation and growth of graphene on the Cu foil, consistently with the results achieved without plasmas.[18] This also suggests an ultra-fast growth of 3D networks of dispersed VGs on a continuous horizontal graphenes film which was observed within 20 seconds of CH_4 exposure. The substrate temperature during the 3 min-long growth of T-GMW films remained below 270 °C. An estimate (Section S1, Supporting Information) suggests that our process is at least 50% and 79% more energy-efficient than previously reported plasma CVD and conventional thermal CVD processes for the deposition of vertical

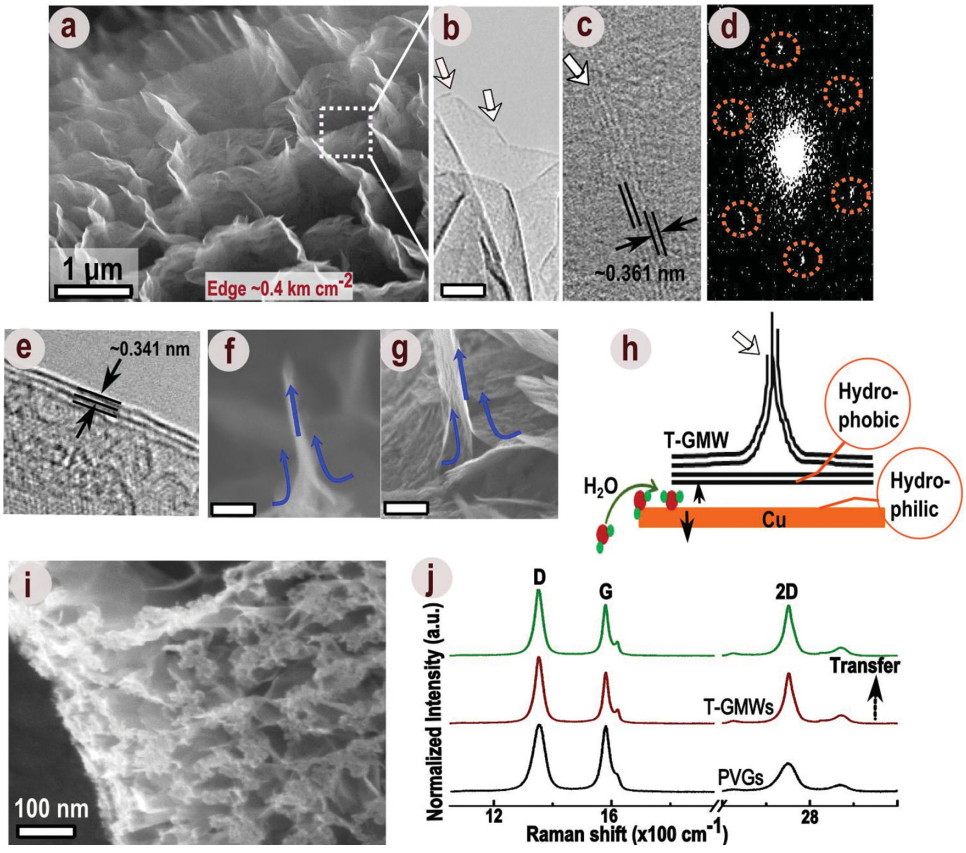

Figure 3. Structrual properties (a-h) and decoupling mechanism (g) of T-GMW films. a) An angle-view SEM image shows that the petal-like vertical graphene sheets in a T-GMW film are structurally connected to each other and form micro/sub-micrometer-sized containers. b–d) A LR-TEM image (b) shows the edges of PVG sheets and a HR image (c) reveals that the vertical sheets are as thin as only 4 graphene layers and their inter-planar spacing is ~0.361 nm which indicates a weak inter-planar interaction. These planes terminate one after another (shown by a white arrow mark) and expose highly reactive open edge planes. The selected-area eletron diffraction (SAED) pattern (d) also confirms the few-graphene-layer crystalline structure of the vertical sheets. e) An HR-TEM image shows only 3 graphene layers in a horizontal graphene film at an early stage of deposition. f–g) The images reveal that a vertical graphene layer forms from native curled parts of two adjacent horizontal graphene layers which coalesce with each other (f) and grow vertically higher in the direction of the electric field in the plasma sheath. The PVG sheets are thinner (f) and thicker (g) when lower and higher methane concentrations are used during the deposition process, respectively. h) Schematic shows the side-view of the T-GMW structure. When the Cu foil is dipped into water, H_2O molecules intercalate and diffuse between the hydrophobic T-GMW film and the hydrophilic Cu surface and decouple the film from the foil. Due to gravity, the Cu foil sinks and the film is lifted-off and floats on the water surface. The white arrow mark shows the terminated graphene edge plane in the schematic of a T-GMW structure. j) Raman spectra reveal that the change in the T-GMW spectrum before and after the transfer process is almost negligible. A Raman spectrum of PVG film is also shown. i) An SEM image of a PVG film. Unless specified, scale bars are 50 nm.

graphene nanosheets and graphene films, respectively, where usually the substrate is heated up to an elevated temperture (>800 °C) and the whole process likely takes more than 20 minutes.

After the deposition process, when the Cu foil was submerged in DI water, the T-GMW film instantly decoupled from the foil and lifted-off onto the water surface (Figure 2b). The film was then transferred onto a polyethylene (PET) sheet, which exhibited almost 76% transparency at an optical wavelength of 550 nm (Figure 2c). The Cu foil was re-used many times to produce transferrable T-GMW films of similar quality (Section S2, Supporting Information). Due to the highly integrated structure of the T-GMWs, no polymeric coating was used during the transfer process. Remarkably, the mophology of T-GMWs on PET was almost unaltered even after bending several times at 1 mm radius of curvature (Figure 2d). Thus, well-integrated, optically transparent T-GMW films applicable for transparent, flexible and lightweight nanodevices have been achieved.

2.2. Structural Integration of T-GMWs

Figure 3a (an angle-view scanning electron microscopy (SEM) image) shows the structural integration among the vertical petal-like graphene layers in a T-GMW film on a PET sheet after the transfer process. These inter-connected layers together form micrometer/sub-micrometer cup-like features, which form compartmentalized containers for very small quantities of biological or chemical substances (discussed later). A high-resolution SEM image (Figure 3b) shows that these graphene layers become thinner and almost transparent towards the top edges. Further, the transmission electron microscopy (TEM) analyses reveal that the top of T-GMW structures consist of 3-4 layers of graphene with an interlayer distance of ~0.361 nm which is larger than in graphite (Figure 3c). This suggests a weaker bonding among the layers; moreover, the individual graphene sheets terminate one after another, creating thinner petal-like sheets as well as the open graphene edge planes (as indicated by arrows in Figure 3b,c). Thus, the produced T-GMWs consist of a high density of open planes (>400 m/cm^2) and, depending on their zig-zag and/or armchair[19] configuration, they possess a higher localized density of states near the Fermi-level[8] and exhibit higher surface activity compared to a graphene basal plane. The electron diffraction pattern (Figure 3d) also confirms a few graphene layers in the T-GMW film.

Further analyses were performed to reveal the stuctural integration between the horizontal and vertical graphene layers in the T-GMW film. A TEM image in Figure 3e shows only 3 graphene layers in the deposited horizontal graphene at early stage of deposition. Figure 3f,g shows that the two neighboring graphene layers parallel to the substrate surface are curled up to form a vertical nanosheet. This suggests that horizontal graphene layers are first deposited on the Cu substrate due to the catalytic effect[14] and the top few layers on the horizontal graphene film curl up possibly due to the plasma-specific effect of the vertical electric field and the enhanced mobility of carbon-based building units in the direction of the electric field.[20,21] After detaching from the underlaying graphene layers, they extend and grow upwards in a vertical direction in the presence of continuous delivery of carbon species,[22] then coalesce with neighboring curled graphene sheets and form petal-like vertical nanosheets (as sketched in Figure 3h). Further, these petal-like vertical graphene sheets coalesce with neighboring nanosheets and form a 3D network. Thus, the vertically stacked graphene layers are a native part of (partially) horizontally stacked layers with upward bending. Such integration provides not only a very reliable mechanical stablility but also an efficient electron transport from the vertical sheets that seemlessly flow into the horizontal graphene layers thereby forming a very-low-resistivity path for the elecron current. This stacking of graphene sheets features a much lower resistance compared to the hybrid structures with a large number of defects and interfaces.

The thickness of the petal-like vertical graphene nanosheets is controlled by the concentration of H_2 with respect to CH_4 (in terms of partial pressure) in the gas mixture. As two graphene layers coalesce with each other, the nanosheets in the vertical growth direction (due to localized electric field of the plasma sheath) become thinner (3-4 graphene layers) as they grow further under conditions of a high partial pressure of H_2 (concentration was >70%) in gas mixture during the deposition process (Figure 3f). This could be attributed to dominant sheet-thickness-dependent fast etching[23] and staturation of the outer grapehene layer by the impinging hydrogen species. As the CH_4 concentration is increased, the delivery of carbon species increases rapidly which not only causes a higher growth rate but also thicker nanosheets (Figure 3g, Section S3 in Supporting Information). However, the partial pressure of argon in the gas mixture also played an important role in the T-GMW growth. We observed the growth of PVG films without any continuous graphene film underneath (Figure 3i) when the Ar concentration in the gas mixture was relatively high (>20%). This is likely due to the damage to the initially deposited horizontal graphene layers caused by excessive Ar^+ ion bombardment, which creates defect sites from which the vertical graphene nanosheets eventually grow.[6,24] With the increased partial pressure of CH_4 in terms of concentration in the gas mixture, the impingement rate of carbon species on the substrate surface increases which leads to the observed high growth rate. However, it also increases the number of sp^3 defects in the graphene film. Therefore, the interplay between the impingement rate of carbon species and the growth and etching rates of the graphene film is crucial for the effective control of the thickness and quality of the VGs.

2.3. Water-Assisted Decoupling

The surface energy of the Cu substrate was strongly affected by the H_2 + Ar plasma exposure which modified its surface wetting properties. The wettability of the Cu surface was effectively changed from low hydrophobic (water contact angle ~70°) to hydrophilic (~6°) when it was exposed to the H_2 + Ar plasma. However, the deposited T-GMW film remained hydrophobic (contact angle ~120°) (Figure 3h). This suggests that the Cu surface interacts strongly with water after the deposition process, while the bottom layer of the T-GMW film is in weak interaction with water. As the substrate is dipped into water

at room temperature, water molecules are likely to intercalate and quickly diffuse[25] between the film and the copper surface (Figure 3h). This substantially reduces the weak T-GMW-copper bond by the screening effect and decouples the film from the substrate. Further, the copper foil sinks in water due to gravity and the GMW film is lifted-off onto the water surface (indicated by black arrow marks in Figure 2b, 3h). Then, the film floating on water is lifted onto a targeted substrate. The relatively high wettability of the Cu foil, likely responsible for the T-GMW film detachment, is considered to originate from the change in its nanoscale crystallographic features (Figure 2a) which mostly occurs during the H_2 + Ar plasma treatment. This was further confirmed by depositing PVG films on the Cu foil just after a few seconds of the H_2 + Ar plasma treatment or directly exposing the Cu foil to the CH_4 + H_2 +Ar plasmas. In these cases, the observed change in wettability of Cu foil was very small and the film did not decouple from the Cu surface when it was submerged in DI water. The change in nanoscale crystallographic features on the Cu foil in these processes is relatively small due to the significant carbon species impingement and graphene film growth on the surface. However, we cannot rule out some other factors in addition to the observed changes in crystallographic features that may also cause the lift-off process, which are currently under investigations. We also observed that the water-assisted decoupling and transfer process is not affected by the number of graphene layer in the film (Section S3, Supporting Information).

We emphasize that our decoupling and transfer process does not require either a coating of carrier material or solvent-rinsing which could damage the 3D vertical networks. The vertical networks remained robust during decoupling and after the transfer to chemically diverse surfaces. This is attributed to the structural integrity of the T-GMW networks where vertical petal-like nanosheets are a native part of the horizontal graphene film and are simultaneously interconnected to each other. A sheer force[26] exerted on the film during the lift-off and transfer process is likely to be distributed among the vertical inter-connections and a tendency to scroll up is easily avoided even in the absence of the carrier material coating. Further, the copper substrate was again used for deposition of similar-quality T-GMWs (See Supporting Information, Section S2). Thus, the approach for decoupling and transferring the deposited graphene films is instant, more cost-effective and extremely environmentally friendly compared to the previously reported methods. A more detailed analysis for a horizontal graphene film will be reported separately.

The structural quality and integrity of T-GMW films were further analyzed and confirmed by collecting micro-Raman spectra (Figure 3j) from the film before and after the transfer process. The graphitic G-peak at 1579 cm^{-1} is associated with the doubly degenerated phonon mode at the Brillouin zone center. However, the 2D-peak at 2702 cm^{-1} corresponding to second-order phonon scattering at the zone boundary with a broad full width at half maximum (FWHM) of 41cm^{-1} suggests misoriented out-of-plane stackings in few graphene layers.[27,28] This also indicates the weaker interaction between stacked layers and larger interplanar distance than in graphite, as also shown by the TEM image (Figure 3c). The intensity ratio (I_{2D}/I_G) of ~0.9 further confirms that the T-GMW is composed of only a few graphene layers. There is also a relatively high-intensity disorder-related D-peak at 1352 cm^{-1} in the spectra which is most likely due to the presence of a high density of open graphitic edges and possibly few structural defects in graphene layers. After the transfer process, the intensity ratio and peak position of all peaks did not noticeably change. This suggests that water did not diffuse into the T-GMW film during the transfer process and the structural quality and integrity of the film remained almost unaltered. Figure 3j also shows a Raman spectrum collected from a PVG film without underlaying horizontal graphene layers.

2.4. Functional Properties in Applications

The performance of the T-GMWs was investigated and compared with the PVG films in a realistic flexible, transparent and ultra-light nanodevice configuration. The transferred films were investigated for their electrical properties at different bending curvature and also tested for NO_2 gas sensing. Nitrogen dioxide is a very hazardous gas in the environment and continued or frequent exposure may cause increased incidences of acute respiratory illness. Therefore, its detection at trace levels is very important.

2.4.1. Electrical Transport Properties

The films were transferred onto polyethylene (PET) sheets for their electrical transport measurements. The electrical resistance data for the films were collected at different bending curvature using a two-probe method. **Figure 4**a shows the electrical resistances of the T-GMW and PVG films (at the films transparency of 76%) after 10 cycles of bending to a 1 mm radius of curvature and release. The sheet resistance of T-GMW was measured as ~350 Ohm/cm^2 which is notably lower than any transferred horizontal graphene films produced in PECVD and comparable to the films produced in thermal CVD processes at high temperatures (~1000 °C).[6,16] In comparison, the PVG films show a higher resistance of ~1900 Ohm/cm^2. Upon bending the films (see Figure 2d), the sheet resistance of the T-GMW and PVG films at a bending radius of 1 mm increased up to 410 and 2300 Ohm/cm^2, respectively. We stress that the sheet resistance of horizontal graphene films produced using PECVD is usually >1 kOhm/cm^2,[29] mostly due abundant defect sites which trap the charge carriers. The overall sheet resistance may also increase due to the tunnelling junction effects. In our case, the T-GMW networks are highly integrated and the charge carrier trapping sites, and hence the overall sheet resistance are reduced in both horizontal and vertical graphene layers integrated into the T-GMW structures. This also suggests that the T-GMW films feature higher vertical and horizontal in-plane carrier mobilities. However, we can not neglect the presence of defect sites on the horizontal graphene layers at the bottom of T-GMW which contribute to the film resistance (~350 Ohm/cm^2). While after bending both the T-GMW and PVG films recovered almost 81% and 42% conductivity, respectively, there was only <5% deviation in the film resistance value from the 1st to the 2nd cycle of bending and <0.1% to the 10th

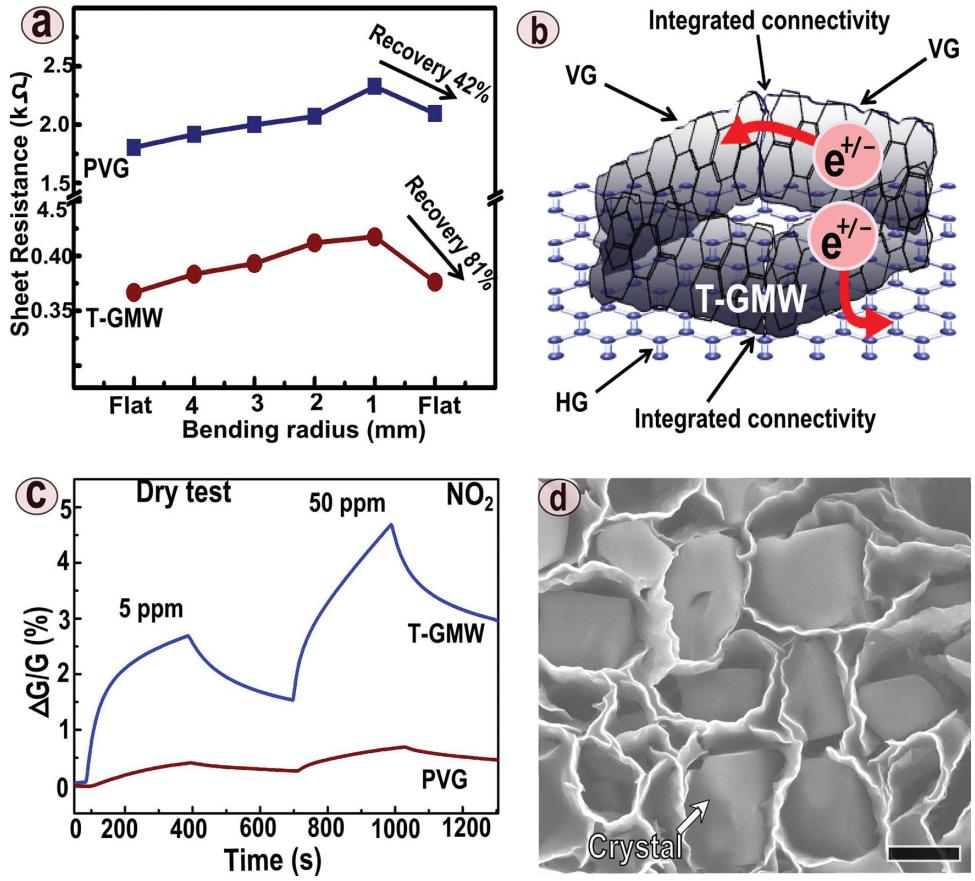

Figure 4. T-GMW nanodevice applications. a–b) The sheet resistance measurements show that (a) T-GMW films recover 81% electrical-conductance while PVG films recover only 42% after the 10th cycle of bending from flat to 1 mm radius of curvature. The significant recovery of the T-GMW films is due to integrated connectivity among the vertically stacked graphene layers as well as between the vertical and horizontal graphene layers (b). c) The gas sensing measurements show that the sensitivity of the T-GMWs for NO_2 gas at room temperature is almost one order of magnitude higher compared to the PVG structures. d) T-GMW as compartmentalized containers for chemial-/bio-species with femto-to-picoliter storage capacity of individual microwells. Individual salt crystals are stored separately.

cycle (not shown here). Thus, the T-GMW films without any external binding materials show a strong potential as a functional transparent and conducting electrode material for next-generation flexible devices.

2.4.2. Gas Sensing Device

For the NO_2 gas sensing, the films were transferred onto mesoporous alumina discs as required for the assembly into a gas sensing device (details in Methods section). All sensitivity of the films were measured in terms of their charge conductance at room temperature using an experimental method reported before.[30] We found that the PVG films showed a detectable response to the NO_2 gas down to about 5 ppm (Figure 4c). When the flow of NO_2 is turned off, the conductance of the film decreases. The conductivity of the sensors increased in response to 5 minutes exposure to 50 ppm concentrations of NO_2. However, the sensitivity of the T-GMW films was almost one order of magnitude higher compared to the PVG films. This also suggests that the defects in the T-GMWs are minimal leading to fast charge transport between the two integrated vertical graphene layers and along the horizontal and vertical graphene layers (Figure 4b). This charge transfer is affected by a small amount of ad-molecules being sensed. However, in the PVG films, the charge carriers are trapped at the junctions and/or defect sites. In this case, adsorption of gas molecules has a weaker effect on the electron transport which results in the relatively lower sensitivity of the PVG-based sensors. Thus, the T-GMW films represent highly performing functional materials for the nanodevices operated in dry environments.

2.4.3. Transparent Micro-Container Wells

To demonstrate the applicability of micro-well structures of the T-GMW film as micro-containers, phosphate buffered saline (PBS) solution was dropped on the film. The PBS solution was chosen as it is a buffer solution commonly used in biological research. After the drop-dry, we observed that the salt crystals are formed and compartmentalized in individual micro-wells regardless of the micro-well shapes (Figure 4d). The estimated average volume of the crystals contained within the micro-wells in Figure 4d was approximately 200 femto-liters. Thus, the

T-GMWs could indeed be used as transparent micro-containers to store, contain and/or separate biological cells, clusters of proteins, chemicals, etc, with the storage capacity of the micro-well compartments in the pico-to-femto-liter range.

3. Conclusion

In summary, we have developed a plasma-enabled, potentially scalable synthesis process for wet-chemical-/binder-free, structurally integrated vertical graphene networks on cheap polycrystalline Cu foils. We have also demonstrated, for the first time, that both the T-GMW and PVG networks may be instantly decoupled and transfered from the foil to virtually any chemically diverse nanodevice platform, without any hazardous chemicals. These 3D networks in form of T-GMWs are not only optically transparent (76% at 550 nm wavelength) with a high density of (>400 m/cm^2) reactive open graphitic edges, but also retain unaltered mechanical and structural integrity upon repeated large mechanical deformations. These films exhibit excellent sensing properties in dry environment for very hazardous NO_2 gas and also demonstrate their pico-to-femtoliter storage capacity of individual salt nanocrystals. These findings are promising for the applications of the "third-generation" (T-GMWs) vertical graphenes in a range of high-performance flexible, transparent, and ultra-light nanodevices. These applications are also expected to complement and expand more traditional applications of vertical graphenes in energy storage devices.[31,32]

4. Experimental Section

Plasma-Enabled Growth Process: Polycrystalline Cu foils (dominated by (100) plane) of 0.125 mm thickness were used as substrates. The foils were cleaned by gently washing with ethanol to remove any surface contamination and were then loaded into an inductively coupled plasma CVD reactor. After achieving a high-vacuum environment (~1×10^{-4} Pa), the foil was exposed to a plasma discharge in a mixture of Ar and H_2 gases (ratio 1:3) for 1.5 minutes and then CH_4 gas was let in for 3 minutes for T-GMW film deposition. Details of the process are mentiond in Supporting Information S4.

Microscopy and Microanalysis: The VG films were characterized by SEM (Zeiss Auriga field-emission SEM, operated at 5 kV) equipped with EBSD (NordlysNano EBSD detector, Oxford Instruments) and TEM (JEOL 3000F, operated at 300 kV). Micro-Raman spectra were collected at room temperature using a Renishaw *in*Via confocal Raman spectroscope (with a laser source 514 nm).

Gas Sensing Devices: Gas sensing measurements were performed using the device sketched in Figure S4. Two separate sensing platforms were fabricated by transferring the T-GMW and PVG films on porous anodic alumina templates (average pore diameter ~200 nm) and attaching two electrodes (6.0 mm apart) onto each platform. A chemiresistor platform was prepared by cutting a sample of the size of 5 mm × 3 mm and attaching it to a filament holder using Ag epoxy. The platform was then inserted into the sensing device with a gas chamber volume of ~60 cm^3. Dry nitrogen was used as a buffer gas. A mixture of 50 ppm NO_2 in nitrogen (Spectra Seal, BOC Limited) was used in appropriate mixture with pure dry nitrogen buffer gas to obtain NO_2 concentration to reduce from 50 to 5 ppm. The electrical resistivity measurements were performed using a picoammeter (Keithley 6487) and the current limit was set at 10 nA to minimize/avoid Joule heating of the sample.

Transparent Micro-Container Systems: A single droplet of Dubleco's PBS solution (D8662, purchased from Sigma-Aldrich) dropped onto a T-GMW film was dried in open environment for 4 hours. Salt crystals formed from PBS within individual micro-well compartments were characterized using SEM.

Supporting Information

Supporting Information is available from the Wiley Online Library or from the author.

Acknowledgements

Authors thank J. H. Fang for assistance in TEM imaging and I. Levchenko for fruitful discussions. This work was partially supported by CSIRO and the Australian Research Council. T.v.d.L. acknowledges support by a CSIRO OCE top-up scholarship and an APA award from the University of Sydney.

Received: March 28, 2014
Revised: June 29, 2014
Published online: August 19, 2014

[1] T. Georgiou, R. Jalil, B. D. Belle, L. Britnell, R. V. Gorbachev, S. V. Morozov, Y.-J. Kim, A. Gholinia, S. J. Haigh, O. Makarovsky, L. Eaves, L. A. Ponomarenko, A. K. Geim, K. Novoselova, A. Mishchenko, *Nat. Nanotechnol.* **2013**, *8*, 100.
[2] I. Khrapach, F. Withers, T. H. Bointon, D. K. Polyushkin, W. L. Barnes, S. Russo, M. F. Cracium, *Adv. Mater.* **2012**, *24*, 2844.
[3] F. Bonaccorso, Z. Sun, T. Hasan, A. C. Ferrari, *Nat. Photon.* **2010**, *4*, 611.
[4] S. De, P. J. King, M. Lotya, A. O'Neill, E. M. Doherty, Y. Hernandez, G. S. Duesberg, J. N. Coleman, *Small* **2010**, *6*, 458.
[5] J. C. Claussen, A. Kumar, D. B. Jaroch, M. H. Khawaja, A. B. Hibbard, D. M. Porterfield, T. S. Fisher, *Adv. Func. Mater.* **2012**, *22*, 3399.
[6] L. Jiang, T. Yang, F. Liu, J. Dong, Z. Yao, C. Shen, S. Deng, N. Xu, Y. Liu, H.-J. Gao, *Adv. Mater.* **2013**, *25*, 250.
[7] J. R. Miller, R. A. Outlaw, B. C. Holloway, *Science* **2010**, *329*, 1637.
[8] N. G. Shang, P. Papakonstantinou, M. McMullan, M. Chu, A. Stamboulis, A. Potenza, S. S. Dhesi, H. Marchetto, *Adv. Func. Mater.* **2008**, *18*, 3506.
[9] L. Qiu, J. Z. Liu, S. L. Y. Chang, Y. Wu, D. Li, *Nat. Commun.* **2012**, *3*, 1241.
[10] Y. Xu, K. Sheng, C. Li, G. Shi, *ACS Nano* **2010**, *4*, 4324.
[11] K. Davani, M. Shaygan, N. Kheirabi, J. Zhao, D. A. Kovalenko, M. H. Rummeli, J. Optiz, G. Cuniberti, J.-S. Lee, M. Meyyappan, *Carbon* **2014**, *72*, 372.
[12] C. Mattevi, H. Kim, M. Chhowalla, *J. Mater. Chem.* **2011**, *21*, 3324.
[13] L. Gao, G.-X. Ni, Y. Liu, B. Liu, A. H. C. Neto, K. P. Loh, *Nature* **2014**, *505*, 190.
[14] X. Li, W. Cai, J. An, S. Kim, J. Nah, D. Yang, R. Piner, A. Velamakanni, I. Jung, E. Tutuc, S. K. Banerjee, L. Colombo, R. S. Ruoff, *Science* **2009**, *324*, 1312.
[15] T. Yamada, J. Kim, M. Ishihara, M. Hasegawa, *J. Phys. D: Appl. Phys.* **2013**, *46*, 063001.
[16] K. S. Kim, Y. Zhao, H. Jang, S. Y. Lee, J. M. Kim, K. S. Kim, J.-H. Ahn, P. Kim, J.-Y. Choi, B. H. Hong, *Nature* **2009**, *457*, 706.
[17] S. Kumar, H. Mehdipour, K. Ostrikov, *Adv. Mater.* **2013**, *25*, 69.
[18] J. D. Wood, S. W. Schmucker, A. S. Lyons, E. Pop, J. W. Lyding, *Nano Lett.* **2011**, *11*, 4547.

[19] K. Nakada, M. Fujita, G. Dresselhaus, M. S. Dresselhaus, *Phys. Rev. B* **1996**, *54*, 17954.
[20] S. Xu, I. Levchenko, S. Y. Huang, K. Ostrikov, *Appl. Phys. Lett.* **2009**, *95*, 111505.
[21] K. Ostrikov, E. C. Neyts, M. Meyyappan, *Adv. Phys.* **2013**, *62*, 113.
[22] S. Kumar, K. Ostrikov, *Nanoscale* **2011**, *3*, 4296.
[23] G. Diankov, M. Neumann, D. G-Gordon, *ACS Nano* **2013**, *7*, 1324.
[24] J. Zhao, M. Shaygan, J. Eckert, M. Meyyappan, M. H. Rummeli, *Nano Lett.* **2014**, *14*, 3064.
[25] J.-S. Kim, J. S. Choi, M. J. Lee, B. H. Park, D. Bukhvalov, Y.-W. Son, D. Yoon, H. Cheong, J.-N. Yun, Y. Jung, J. Y. Park, M. Salmeron, *Sci. Reports* **2013**, *3*, 2309.
[26] Y. Wang, Y. Zheng, X. Xu, E. Dubuisson, Q. Bao, J. Lu, K. P. Loh, *ACS Nano* **2011**, *5*, 9927.
[27] L. M. Malard, M. A. Pimenta, G. Dresselhaus, M. S. Dresselhaus, *Phys. Rep.* **2009**, *473*, 51.
[28] A. E. Rider, S. Kumar, S. A. Furman, K. Ostrikov, *Chem. Comm.* **2012**, *48*, 2659.
[29] G. Kalita, K. Wakita, M. Umeno, *RSC Advances* **2012**, *2*, 2815.
[30] L. K. Randeniya, P. J. Martin, A. Bendavid, J. McDonnell, *Carbon* **2011**, *49*, 5265.
[31] D. H. Seo, Z. J. Han, S. Kumar, K. Ostrikov, *Adv. Energy Mater.* **2013**, *3*, 1316.
[32] Z. Bo, W. G. Zhu, W. Ma, Z. H. Wen, X. R. Shuai, J. H. Chen, X. L. Feng, J. H. Yan, K. F. Cen, *Adv. Mater.* **2013**, *25*, 5799.